Normal Modes in Model Jammed Systems in Three Dimensions

Leonardo E. Silbert[1], Andrea J. Liu[2], and Sidney R. Nagel[3]
[1]*Department of Physics, Southern Illinois University, Carbondale, IL 62901, U.S.A.*
[2]*Department of Physics and Astronomy, University of Pennsylvania, Philadelphia, PA 19104, U.S.A. and*
[3]*James Franck Institute, University of Chicago, Chicago, IL 60637, U.S.A.*
(Dated: March 18, 2008)

Vibrational spectra and normal modes of mechanically stable particle packings in three dimensions are analyzed over a range of compressions, from near the jamming transition, where the packings lose their rigidity, to far above it. At high frequency, the normal modes are localized at all compressions. At low frequency, the nature of the modes depends somewhat on compression. At large compressions, far from the transition, the lowest-frequency normal modes have some plane-wave character, though less than one would expect for a crystalline or isotropic solid. At low compressions near the jamming transition, the lowest-frequency modes are neither plane-wave-like nor localized. We characterize these differences, highlighting the unusual dispersion behavior that emerges for marginally jammed solids.

PACS numbers: 81.05.Rm, 83.80.Iz, 63.50.+x, 64.70.Pf,

It is well recognized that the high-frequency vibrations in amorphous materials are strikingly different from those in crystals. In glasses and other amorphous solids, the highest-frequency normal modes are localized in space, while in crystals they are extended excitations [1, 2, 3]. It is also appreciated that even at low frequencies the normal modes of disordered systems can be dramatically different from the long-wavelength plane waves found in ordered materials. The vibrational spectra of amorphous solids are characterized by "boson peaks" – extra low-frequency modes beyond the long-wavelength plane-wave phonons found in crystals. The anomalous modes that fall within the boson peak are believed to be responsible for the unusual low-temperature properties of glasses, such as the plateau in the thermal conductivity [4].

Nowhere are the excess low-frequency excitations more apparent than in a marginally jammed solid, in which a system of particles is compressed to the point where they first begin to touch and form a rigid structure [5, 6, 7, 8, 9, 10, 11, 12, 13]. In this system, the density of normal modes, instead of vanishing as the frequency is lowered towards zero, as in a crystal, remains constant as shown in Fig. 1(a). This leads to an excess in the density of states that *diverges* at zero frequency. This divergence has been interpreted as a boson peak [8]. Thus, one might expect the marginally jammed solid to provide the clearest window into the anomalous low-frequency normal modes characteristic of all amorphous solids.

Previously, we have found that the characteristic frequency and size of the boson peak can be tuned systematically by compressing the marginally jammed solid to higher packing fractions [8]. In the present paper we analyze the structure of the normal modes of disordered packings in three dimensions ($3D$) in the marginally jammed state and at compressions above this state. The system we study here is identical to the one used previously to calculate the density of vibrational states [7, 8, 14]. We simulate a $3D$ system of N ($1024 \leq N \leq 10000$) monodisperse soft-spheres of mass m and diameter σ in cubic simulation cells employing periodic boundary conditions. The particles interact via a finite-range, purely repulsive, harmonic potential:

$$V(r) = \left\{ \begin{array}{ll} V_0(1-r/\sigma)^2 & r < \sigma \\ 0 & r \geq \sigma \end{array} \right\} \qquad (1)$$

where r is the center-to-center distance between two particles. Length and time are measured in units of σ and $(md^2/V_0)^{1/2}$ respectively. We initially place N particles at random in a cubic box of linear dimension L. This corresponds to a $T = \infty$ configuration. We use conjugate-gradient energy minimization [15] in order to obtain $T = 0$ configurations. In order to show visualizations of the normal modes, we have also studied $N = 10000$, bidisperse, 50:50 mixtures of harmonic discs with a diameter ratio of 1.4 in $2D$.

The onset of jamming in the limit of large N occurs at a packing fraction, $\phi_c^\infty = 0.639 \pm 0.003$, and is characterized by the onset of a nonzero pressure. We determine ϕ_c for each of our finite-system initial configurations by incrementally compressing (decompressing) until the pressure just becomes nonzero (just reaches zero). We then compress the system to obtain zero-temperature compressed configurations at controlled values of $\phi - \phi_c$. For each of these configurations, we compute and diagonalize the dynamical matrix [16]. The eigenvalues and eigenmodes of this matrix are respectively the squared frequencies, ω^2, of the normal modes of vibration and the corresponding polarizations $\mathbf{e}_{i_\omega}$ of each particle i in the normal mode of frequency ω.

In a previous paper [8], we analyzed the density of vibrational states $D(\omega)$, of configurations above the jamming threshold, for systems at $\phi > \phi_c$, and found three characteristic regimes, as labeled in Fig. 1(b). In regime A, $D(\omega)$ decreases towards zero as $\omega \to 0$. In regime B (including B' in Fig. 1(a)), $D(\omega)$ is approximately constant, very different than for crystals. Finally, in regime C at high frequencies, $D(\omega)$ decreases with increasing

frequency. Figure 1(a-c) show how the different regimes shift with increasing compression. At high $\Delta\phi \equiv \phi - \phi_c$, regime A extends to fairly high frequencies and regime B is small. As the system is decompressed towards the marginally jammed solid at $\Delta\phi = 0$, regime A shrinks and regime B grows, extending all the way down to zero frequency, as indicated by B' in Fig. 1(a), while regime C remains approximately the same. The growth of regime B at the expense of regime A with decreasing compression signals the proliferation of anomalous low-frequency modes. These are the modes whose structure we wish to understand.

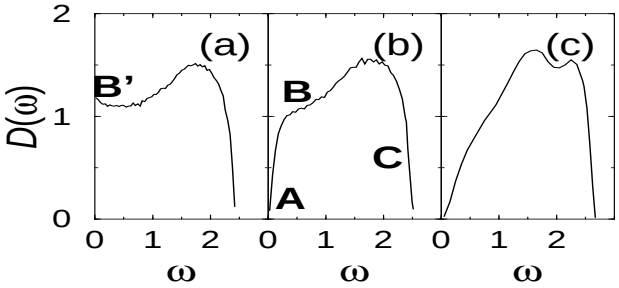

FIG. 1: Density of states $\mathcal{D}(\omega)$ of $3D$ jammed packings with $N = 1024$ monodisperse spheres at three different compressions: (a) $\Delta\phi = 10^{-6}$, (b) $\Delta\phi = 10^{-2}$, and (c) $\Delta\phi = 10^{-1}$. In (a) we identify regime B', and in (b) we identify the regimes A,B, and C, discussed in the text.

In order to visualize the nature of the modes, we turn to the bidisperse 2D system. Fig. 2 shows typical normal modes from regimes A, B', B, and C, defined in Fig. 1(a) and (b). In the left panels, the polarization vector for each particle is shown, while in the right panel, each particle is shaded according to the magnitude of its polarization vector. The mode from regime A, Fig. 2(top), appears to have some plane-wave-like character, although contributions from several different wavevectors are readily apparent. The high-frequency mode corresponding to regime C, Fig. 2(bottom) is quite localized. This particular mode is representative of the high-frequency modes at all values of $\Delta\phi$; visualizations for different $\Delta\phi$ are indistinguishable from that shown in Fig. 2(bottom).

The modes from regimes B' and B, Fig. 2(middle), are neither plane-wave-like nor localized. The right panels more clearly reveal the filamentary nature of the extended vibrational modes in regimes B' and B. Here we point out that these visualizations already suggest some subtle differences between regimes B' and B which we quantify below (see Fig. 7 and related discussion).

Fig. 2 suggests that the modes from both regimes A and B are extended. To analyze directly how extended each mode is, we calculate the inverse participation ratio,

$$P^{-1} = \frac{\sum_{i=1}^{N} |\mathbf{e}_{i_\omega} \cdot \mathbf{e}_{i_\omega}|^2}{\left|\sum_{i=1}^{N} \mathbf{e}_{i_\omega} \cdot \mathbf{e}_{i_\omega}\right|^2}. \qquad (2)$$

Here $\mathbf{e}_{i_\omega}$ is the polarization vector of particle i in the mode ω. We show the results for $\Delta\phi = 10^{-6}$, $\Delta\phi = 10^{-3}$, and $\Delta\phi = 10^{-1}$ in Fig. 3. We find that on a log-log scale, the participation ratio looks quite similar for values of $\Delta\phi$ up to at least $\Delta\phi \approx 10^{-3}$. For high compressions ($\Delta\phi = 0.1$ and higher), P^{-1} at the very highest frequencies (regime C) appears to decrease with increasing compression, but P^{-1} is still large in regime

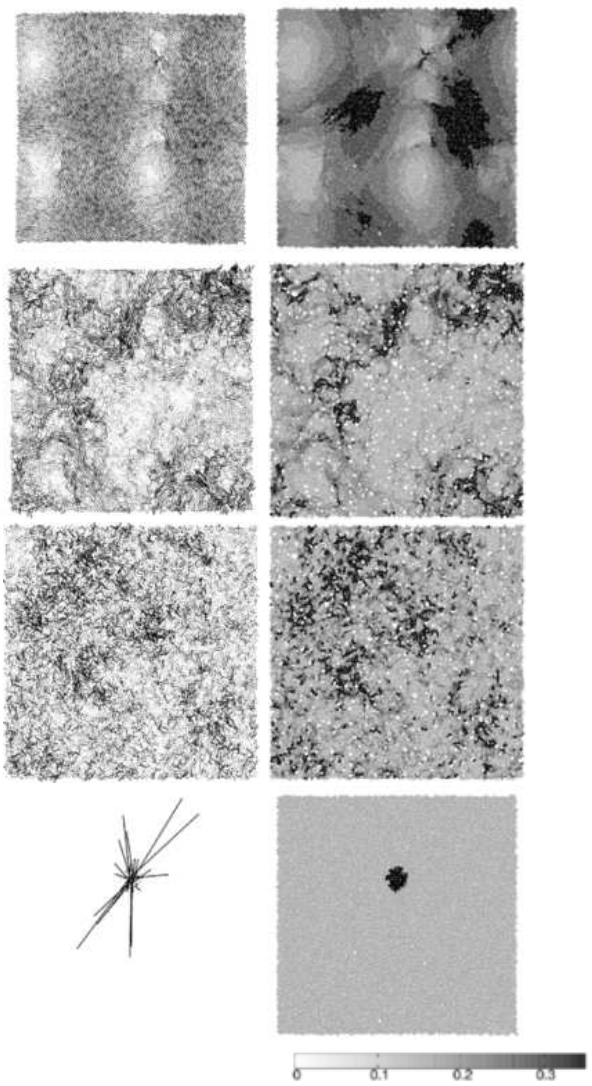

FIG. 2: Normal modes of a $2D$ jammed packing of a 50:50 mix of $N = 10000$ bidisperse disks, with size ratio $1 : 1.4$, interacting with the potential defined in Eq. 1. These figures correspond to the regimes identified in Fig. 1(a),(b) characterized by $(\Delta\phi, \omega)$. Top row panels: Regime A $(1\times10^{-1}, 1.76\times10^{-2})$. Second row: Regime B' $(1 \times 10^{-6}, 3.35 \times 10^{-4})$. Third row: Regime B $(1 \times 10^{-6}, 0.3)$. Bottom row: Regime C $(1 \times 10^{-1}, 2.30)$. Left panels: black lines represent the amplitude and direction of the particle vibrations in that mode. Right panels: particles are shaded according to the magnitude of their polarization vector. The scale bar indicates that darker shading corresponds to a larger ratio of the amplitude to the maximum amplitude of particle displacement in that mode. Particles with no contact neighbors are not shown.

C at all compressions. Thus, the modes in regime C are localized at all compressions. At lower frequencies, however, up to $\omega \approx 2$, we find $P^{-1} << 1$, indicating that the modes are extended over the size of the system. Thus, modes in regimes A and B are extended, while those in regime C are localized.

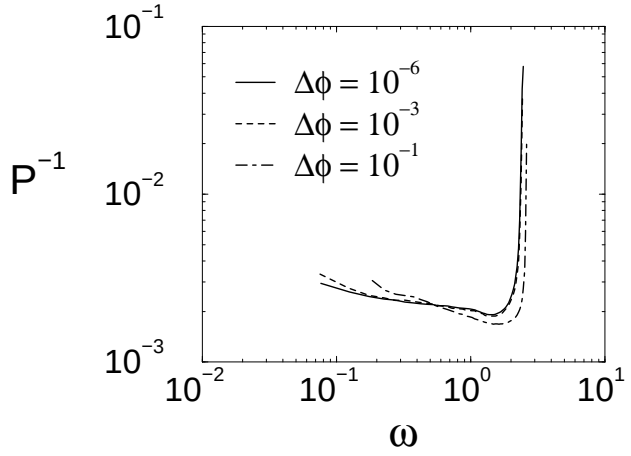

FIG. 3: Inverse participation ratio, P^{-1}, for $3D$ jammed packings of $N = 1024$ monodisperse spheres, at three compressions.

For these jammed, mechanically stable packings, there exist local correlations in the force constants that constitute the dynamical matrix: The forces around each and every particle must be locally balanced. Upon analyzing the spacings $\Delta\omega = \omega_{j+1} - \omega_j$, between successive normal mode frequencies, we find level-repulsion in the distribution of level spacings, $P(s)$, where we define $s = \frac{\Delta\omega}{<\Delta\omega>}$, as the level spacing normalized by the average $< \Delta\omega >$. The distributions shown in Fig. 4 show little dependence on distance to the jamming threshold, and are described quite well by the Wigner-Dyson distribution [17],

$$P(s) = \frac{\pi s}{2} e^{-\pi s^2/4}. \tag{3}$$

The distributions shown in Fig. 4 are peaked around the average spacing and indicate level repulsion by the linear behavior at small spacing. Thus, even though the dynamical matrix is sparse, due to the short-range nature of the interaction potential, the level spacings are not completely random, which would lead to a Poisson distribution, nor are they completely correlated [18].

Another way to characterize the modes is to look at local correlations of the polarizations of neighboring particles. We calculate a quantity, $\cos\theta_e$, that is similar to the phase quotient parameter often probed in glasses [19],

$$\cos\theta_e(\omega) = \frac{1}{N_{\rm pairs}} \sum_{i,j} \hat{\mathbf{e}}_{i_\omega} \cdot \hat{\mathbf{e}}_{j_\omega} \tag{4}$$

where the sum only runs over the number of pairs of particles that interact with each other, $N_{\rm pairs}$, and the

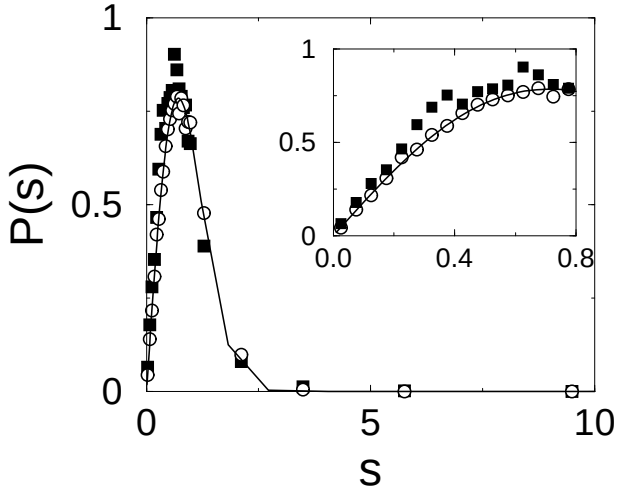

FIG. 4: Distribution, $P(s)$, of level spacings, s, normalized by the the average level spacing, at $\Delta\phi = 10^{-1}$ (■) and 10^{-6} (○) in 3D. Inset shows the linear behavior at small s. The line is a fit to the Wigner-Dyson function of Eq. 3.

normalized polarization vector of particle i associated with the normal mode of frequency ω, $\hat{\mathbf{e}}_{i_\omega} = \frac{\mathbf{e}_{i_\omega}}{|\mathbf{e}_{i_\omega}|}$. For a mode in which every particle is vibrating in approximately the same direction, i.e., strongly correlated motion, one would expect $\cos\theta_e \approx 1$. Figure 5 shows $\cos\theta_e$ as a function of frequency at three values of $\Delta\phi$. Up to compressions of order $\Delta\phi = 10^{-3}$, the behavior of $\cos\theta_e$ with ω is insensitive to compression. Over that range of compressions, $\cos\theta_e$ decreases linearly with frequency, showing that in the low-frequency modes, particle displacements are more correlated with their neighbors and in high frequency modes, particle displacements are more anti-correlated with their neighbors. Note that the frequency ranges of regimes A and B change appreciably with $\Delta\phi$, while $\cos\theta_e(\omega)$ does not; this suggests that the correlations are not noticeably different in the two regimes. At high compressions, the curve begins to show a kink at approximately $\omega = 1.75$ (the boundary between regimes B and C).

As noted earlier (and by visual inspection of the $2D$ modes of Fig. 2), the low-frequency modes both near and far from the jamming threshold appear to have somewhat different character. We have argued that compressed systems away from the jamming threshold contain low-frequency modes that are more plane-wave-like, whereas near the jamming transition, these extended modes are very different from plane waves. At intermediate and high frequencies the modes appear relatively insensitive to packing fraction. In an effort to further differentiate between the nature of the low-frequency modes we measure the spatial extent of correlated vibrational motions. For each mode of frequency ω, we compute the correlation of polarization vectors between particles i and j,

$$\mathcal{C}(r_{ij}) = \langle \hat{\mathbf{e}}(\mathbf{r}_i) \cdot \hat{\mathbf{e}}(\mathbf{r}_j) \rangle \,. \tag{5}$$

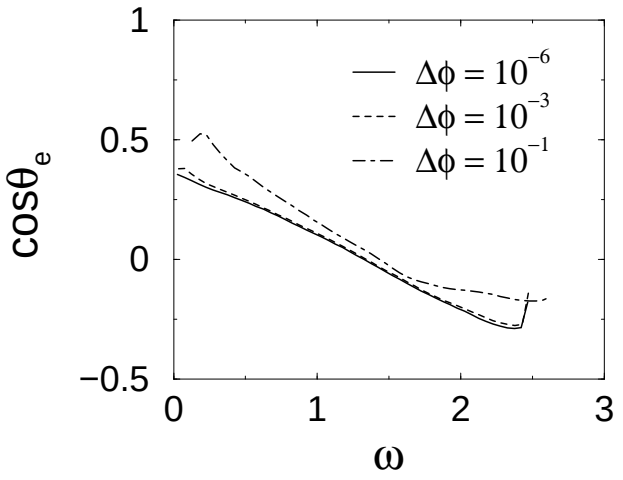

FIG. 5: Correlation between particle displacements in a mode, measured using $\cos\theta_e$ defined by Eq. 4, at three compressions for $3D$ jammed packings with $N = 1024$ monodisperse spheres.

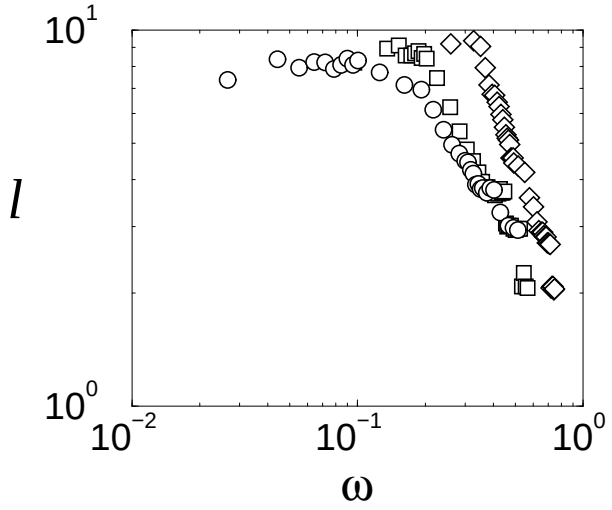

FIG. 7: Dependence of the characteristic length scale ℓ, defined in text, on the normal mode frequency ω, at three values of $\Delta\phi = 10^{-6}$ (◯), 10^{-3} (□), and 10^{-1} (◇), for $N = 10000$ monodisperse spheres in $3D$.

In Fig. 6 we show $\mathcal{C}(r)$ for the lowest lying frequency modes at three different compressions, $\Delta\phi = 10^{-6}$, $\Delta\phi = 10^{-2}$, and $\Delta\phi = 10^{-1}$, for our $3D$ jammed packings.

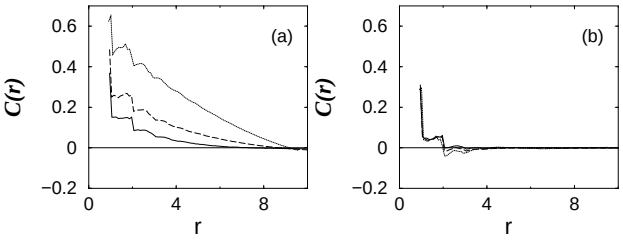

FIG. 6: Spatial correlation function $\mathcal{C}(r)$ of particle vibrations at three values of $\Delta\phi = 10^{-6}$ (solid line), 10^{-2} (dashed), and 10^{-1} (dotted), for $N = 10000$ monodisperse spheres in $3D$. (a) Lowest-lying frequencies, and (b) intermediate frequencies.

For the low-frequency modes we find somewhat stronger correlations at higher compressions. For the middle-to-high frequency range of the vibrational spectrum, beyond regime A, the normal modes become increasingly similar at different compressions. In regime C, the modes are indistinguishable at different compressions.

All of the correlation functions in Fig. 6 decay non-monotonically to zero and cross zero at some finite r. We define the value of r at which $\mathcal{C}(r)$ first crosses zero to be $\ell(\omega)$. In a pure plane wave, particle vibrations are correlated and $\mathcal{C}(r)$ will cross zero at the scale of half the wavelength, so for ordinary sound modes at low frequency, one would expect $\ell(\omega) \propto 1/\omega$. In Fig. 7, we plot ℓ as a function of ω for different $\Delta\phi$ at low-to-intermediate frequencies. For the system closest to the jamming threshold, ℓ is approximately independent of ω at very low frequencies. Beyond this constant region, ℓ decreases with increasing frequency, corresponding to moving along the plateau in the density of states from regime B' to B [20]. As the system moves further from the jamming threshold, i.e., as $\Delta\phi$ increases, the region of constant ℓ shrinks. Over the range of frequencies where ℓ decreases, the characteristic length is greater the further the system is from the jamming threshold. This is to be expected as the modes contain more plane-wave character at larger compressions. At slightly higher frequencies still, the curves begin to overlap, so that the modes do indeed become practically indistinguishable. The frequency at which this occurs coincides with the point in the density of states where the plateau regions start to merge (see Fig. 1 of Ref. 8). These data suggest that the distinction between modes from regimes B' and B is related to how extended the modes are. This is already evident from the visualizations presented in Fig. 2.

Another way to quantify the difference between the extended modes in regimes A and B is through the Fourier transforms of the eigenmodes at different frequencies ω throughout the spectrum. Specifically, we take the Fourier transform of the appropriate component, either longitudinal or transverse, of the particle polarization vector $\mathbf{e}_j(\omega)$, of each particle j [3, 8]:

$$\begin{aligned} f_L(k,\omega) &= \left\langle \tfrac{1}{N} \left| \textstyle\sum_j \hat{\mathbf{k}} \cdot \mathbf{e}_{j\omega} \exp(\imath \mathbf{k} \cdot \mathbf{r}_j) \right|^2 \right\rangle , \\ f_T(k,\omega) &= \left\langle \tfrac{1}{N} \left| \textstyle\sum_j \hat{\mathbf{k}} \wedge \mathbf{e}_{j\omega} \exp(\imath \mathbf{k} \cdot \mathbf{r}_j) \right|^2 \right\rangle . \end{aligned} \tag{6}$$

In a perfect crystal, these functions would be delta-functions at the wavevectors k in each Brillouin zone characterizing the longitudinal or transverse vibrational

modes at frequency ω. In Fig. 8, we show $f_L(k,\omega)$ and $f_T(k,\omega)$ curves for two disordered configurations in three frequency bands: (i) at the lowest frequency, (ii) in the middle of the band, and (iii) at the high-frequency end of the spectrum. Each curve is averaged over a narrow bin of frequencies. For comparison, Figs. 8(a),(b) are from a system very close to the jamming threshold, at $\Delta\phi = 10^{-6}$, and Fig. 8(c),(d) are for a system that is highly compressed and far from the jamming threshold, at $\Delta\phi = 10^{-1}$. At $\Delta\phi = 10^{-6}$, the low and mid-frequency curves correspond to vibrational states in regime B' defined in Fig. 1(a), where the density of states is relatively flat, while the high frequency curve corresponds to regime C. At high compression, $\Delta\phi = 10^{-1}$, the low frequency curve corresponds to a state in regime A, the mid-frequency curve corresponds to regime B and the high frequency curve corresponds to regime C. The longitudinal functions in general show much more pronounced structure than do their transverse counterparts. The only exception to this occurs at very low frequencies and small wavevectors. In this region the transverse function has a very tall first peak and the longitudinal function shows only a hint of structure. The low-wavevector part of the peak in $f_T(k,\omega_{\rm low})$ is not resolved because it occurs at $k < 2\pi/L$ where L is the size of the system. That is, the peak is cut off because of the finite size of the system. The first peak in $f_L(k,\omega_{\rm low})$ is also absent for the same reason. In order to see this structure, one would have to either use a larger box size at the same value of frequency or else look at $f_L(k,\omega)$ at a larger value of ω.

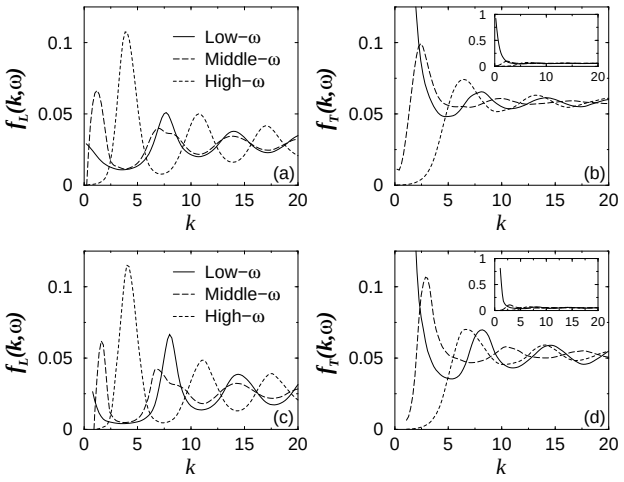

FIG. 8: Fourier transforms of the eigenmodes for the low (solid line), middle (dashed line), and high frequency (dotted line) regions of the vibrational spectrum, at two extreme compressions in 3D. Top panels: $\Delta\phi = 1 \times 10^{-6}$, for the, (a) longitudinal, and (b) the transverse components. Bottom panels: $\Delta\phi = 1 \times 10^{-1}$, for the, (c) longitudinal, and (d) the transverse components. Insets to (b) and (d) show the dominance of the low-k peak in the transverse functions.

There are multiple oscillations visible in the longitudinal response, $f_L(k,\omega)$. This structure can be thought of as the equivalent of the repeated structure seen in the higher Brillouin zones of a crystal [3]. It reflects the large, sharp first peak in the pair-correlation function, $g(r)$ [21], which leads to strong oscillations in the structure factor $S(k) = \langle |\sum_i \exp(\imath \mathbf{k}\cdot\mathbf{r})|^2\rangle$ [7]. Similar oscillations show up but with a much smaller amplitude in $f_T(k,\omega)$.

Overall, the results look fairly similar for the two compressions. For the longitudinal response, the peaks are somewhat smaller and wider at low compression. However, the most obvious difference is not in the peaks but in the minima between them which become more shallow at small $\Delta\phi$. This is particularly apparent at the lower frequencies in the longitudinal response. This means that more wavevectors are making significant contributions to the low-frequency longitudinal modes at low compression (which are in regime B) than to low-frequency longitudinal modes at high compression (which are in regime A), making the mode very different from any plane wave with a single wavevector. A similar trend is apparent in the transverse response. Contributions of wavevectors different from the peak value are relatively larger at low compressions; that is, more wavevectors contribute to eigenmodes in regime B than in regime A. The intermediate wavevector oscillations, clearly visible at $\Delta\phi = 10^{-1}$, are much less pronounced near the onset of jamming. At low frequency, the transverse response is practically flat at wavevectors $k > 5$ – all of these high wavevectors contribute nearly equally in regime B.

The velocity of longitudinal or transverse sound can be estimated from the frequency-dependence of the position of the first peak in $f_L(k,\omega)$ or $f_T(k,\omega)$. Unlike in crystals, the dispersion curve is not well-defined because, as we have seen in Fig. 8, $f_L(k,\omega)$ and $f_T(k,\omega)$ have significant amplitude over a large range of wavevector at all frequencies. As a result, it is not sufficient to simply plot the positions of the peaks of the dynamic structure factors as one might do for a crystal.

To emphasize the idea of mode mixing, the dispersion data are best visualized on a gray scale plot as shown in Fig. 9. (The features outlined here have been seen in a range of glassy systems, including soft-sphere [22], covalent [23], and metallic [24] glasses.) Because the amplitude of the first peak in $f_T(k,\omega)$ is so strong, variations at wavevectors greater than the first peak are lost in Fig. 9. Therefore, to observe the underlying structure in the dispersion data at larger wavevectors, in Fig. 10, we show the transverse dispersion curves over a limited range in amplitude. These nicely contrast the unusual underlying structure to the dispersion relations at the two compressions.

It is clear from looking at these plots that the dispersion relations are very broad indeed, especially at low compression. Moreover, there is very little difference between the two compressions, although the contrast decreases for both transverse and longitudinal modes with decreasing compression. The limit of what we can achieve is $\Delta\phi = 10^{-6}$. It is not clear to us if one were able to go even closer to $\Delta\phi = 0$ whether the variations in $f_T(k,\omega)$

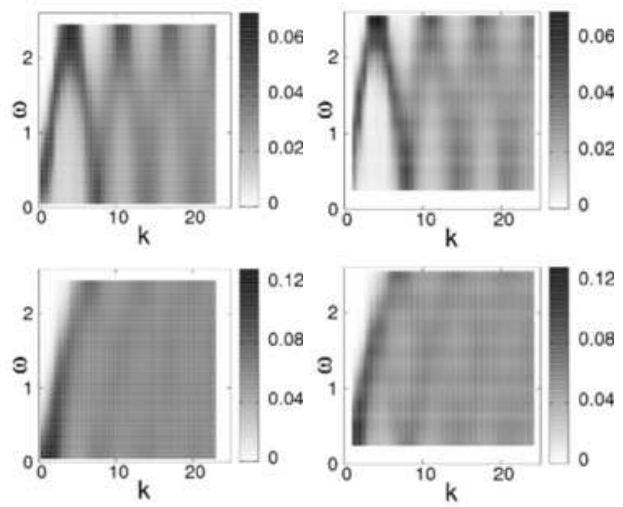

FIG. 9: Dispersion relation at two different compressions in 3D. Left panels: $\Delta\phi = 1\times10^{-6}$. Right panels: $\Delta\phi = 1\times10^{-1}$. Top and bottom panels correspond to longitudinal and transverse modes respectively. Darker shading corresponds to larger amplitude in $f_{L,T}$. The maximum of the transverse amplitudes are typically a factor of 5 larger than the longitudinal data. The bars to the right indicate the amplitude scale.

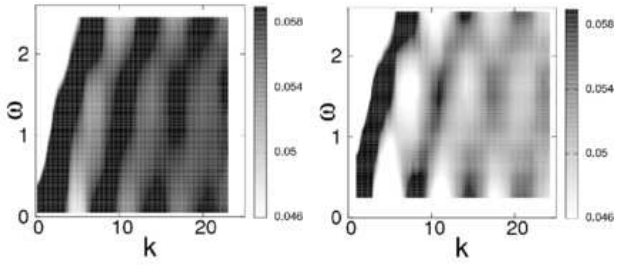

FIG. 10: Transverse dispersion data in 3D for $\Delta\phi = 1\times10^{-6}$ (left) and 1×10^{-1} (right), over a limited range in amplitude f_T (see scale bar).

would disappear entirely.

It is also unclear how to define a proper velocity of sound not only because the peaks in the dispersion relations are so broad, but also because their amplitudes decay rapidly with increasing (k,ω). We illustrate this latter point in Fig. 11 where we show the approximately exponential decay of the maximum peak height of the transverse Fourier modes with increasing frequency. We have been unable to determine precisely whether the decay constant depends on compression; although there appears to be a small difference between the two compressions shown in Fig. 11, that difference is small.

In summary, we have studied the characteristics of vibrational modes in different frequency regimes. From the density of states, we see that there are three regimes: regime A, where the density of states drops towards zero with vanishing frequency; regime B, where the density of

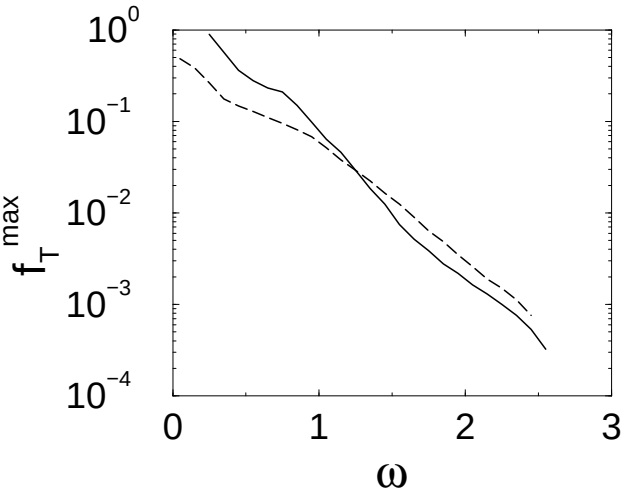

FIG. 11: Decay of the peak maximum of the transverse mode transforms within the first "Brillouin zone", for $\Delta\phi = 10^{-1}$ (solid line) and 10^{-6} (dashed line) in 3D.

states is approximately flat; and regime C, where the density of states is decreasing towards zero with increasing frequency. As the system is decompressed towards the marginally jammed state, regime B (or B') increases at the expense of regime A while regime C is relatively unaffected. Modes from regime C are localized while modes from regime A and B are extended. Those in Regime A are somewhat more plane-wave-like, in that contributions from wavevectors away from the peak of the dynamic structure factor are fairly small (the peak is relatively narrow) while those in Regime B have broader peaks in the dynamic structure factors, with significant contributions from a wider range of wavevectors. Generally, however, we do not observe strong differences between modes from regime B and regime A. Thus, the change in the nature of the modes with decreasing compression is much less dramatic than the change in the density of vibrational states.

Acknowledgments

We thank T. Witten for helpful discussions. We gratefully acknowledge the support of NSF-DMR-0087349 (AJL), NSF MRSEC DMR-0213745 (SRN), DE-FG02-03ER46087 AJL,LES), and DE-FG02-03ER46088 (SRN,LES).

[1] R. J. Bell, in *Methods in Computational Physics: Advances in Research and Applications*, edited by G. Gilat (Academic, New York, 1976), vol. 15, p. 216.

[2] S. John, H. Sompolinsky, and M. J. Stephen, Phys. Rev. B **27**, 5592 (1983).

[3] G. S. Grest, S. R. Nagel, and A. Rahman, Phys. Rev. Lett. **49**, 1271 (1982).

[4] W. A. Phillips, ed., *Amorphous solids, Low temperature properties* (Springer, Berlin, 1981).

[5] D. J. Durian, Phys. Rev. E **55**, 1739 (1997).

[6] C. S. O'Hern, S. A. Langer, A. J. Liu, and S. R. Nagel, Phys. Rev. Lett. **88**, 075507 (2002).

[7] C. S. O'Hern, L. E. Silbert, A. J. Liu, and S. R. Nagel, Phys. Rev. E **68**, 011306 (2003).

[8] L. E. Silbert, A. J. Liu, and S. R. Nagel, Phys. Rev. Lett. **95**, 098301 (2005).

[9] M. Wyart, S. R. Nagel, and T. A. Witten, Europhys. Lett. **72**, 486 (2005).

[10] M. Wyart, L. E. Silbert, S. R. Nagel, and T. A. Witten, Phys. Rev. E **72**, 051306 (2005).

[11] A. R. Abate and D. J. Durian, Phys. Rev. E **74**, 031308 (2006).

[12] E. Somfai, M. van Hecke, W. G. Ellenbroek, K. Shundyak, and W. van Saarloos, Phys. Rev. E **75**, 020301(R) (2007).

[13] T. S. Majmudar, M. Sperl, S. Luding, and R. P. Behringer, Phys. Rev. Lett. **98**, 058001 (2007).

[14] L. E. Silbert, C. S. O'Hern, A. J. Liu, and S. R. Nagel, in *Unifying concepts in granular media and glasses*, edited by A. Coniglio, A. Fierro, H. J. Herrmann, and M. Nicodemi (Elsevier, Amsterdam, 2004), p. 1.

[15] W. H. Press, B. P. Flannery, S. A. Teukolsky, and W. T. Vetterling, *Numerical Recipes in Fortran 77* (Cambridge University Press, New York, 1986).

[16] N. W. Ashcroft and N. D. Mermin, *Solid State Physics* (Brooks/Cole, 1976).

[17] M. L. Mehta, *Random Matrices and the Statistical Theory of Energy Levels* (Academic Press, New York, 1967).

[18] We have recently discovered that the distribution of level spacings has also been calculated by Z. Zeravcic, W. van Saarloos, and D. R. Nelson (unpublished).

[19] P. B. Allen, J. L. Feldman, J. Fabian, and F. Wooten, Philosophical Magazine B **79**, 1715 (1999).

[20] Over the limited range of data, the initial decay approximately follows, $\ell \sim \omega^{-1}$.

[21] L. E. Silbert, A. J. Liu, and S. R. Nagel, Phys. Rev. E **73**, 041304 (2006).

[22] H. R. Schober, J. Phys.:Condens. Matter **16**, S2659 (2004).

[23] O. Pilla, L. Angelani, A. Fontana, J. R. Goncalves, and G. Ruocco, J. Phys.:Condens. Matter **15**, S995 (2003).

[24] J. Hafner, Phys. Rev. B **27**, 678 (1983).